Marker Finding and Automated Registration in AFM-Fluorescence Microscope Hybrid Imaging

Serdar Çakıcı

Abstract

To identify multi-protein complexes with high accuracy, Dr. Tessmer and her group derived a system that uses fluorescence microscopy and atomic force microscopy (AFM) simultaneously on the same specimen. They overlaid images coming from the two different types of microscopes and came up with a hybrid image that had more information about the specimen compared to the information gained from each microscope image alone. Localization of markers in AFM and fluorescence images and overlaying the images using the markers were all done manually in their work. In my work, I developed algorithms to automatically find the markers in both images and register images using the locations of the markers. The manual steps of marker finding and image registration takes many hours for scientists, whereas with the automated version I devised, the same operations take only a few seconds.

1. Introduction

[Tessmer] describes factors that damage DNA and how DNA is repaired afterwards as follows:

"*DNA is damaged continuously by agents that occur naturally within our cells as well as by exogenous factors such as high energy radiation. If unrepaired, this damage can lead to cell death or severe diseases such as cancer. To maintain genomic stability, a number of DNA repair mechanisms have evolved. Each mechanism targets different types of DNA damage and many of them are evolutionarily conserved. One example for a highly conserved DNA repair mechanism is the Nucleotide Excision Repair (NER) system that can recognize and repair a range of different DNA lesions. In an NER system, different protein molecules interact to repair DNA.*"

Atomic Force Microscopy (AFM) is commonly used to study protein-DNA complexes involved in DNA repair at the level of the individual molecules. While AFM imaging in itself is a well-established and extremely powerful technique in single molecule structural studies of protein-protein or protein-DNA complexes, many biological systems involve multi-protein complexes which are often difficult to analyze by AFM imaging alone. In other words, AFM does not have the ability to distinguish different proteins.

To address these issues, [Fronczek et al.] devised a technique based on the integration of high-resolution fluorescence microscopy (by which it is possible to label and distinguish proteins) and AFM. A fluorescence microscope is a type of optical microscope that uses fluorescence to come up with an image of a specimen. Unlike fluorescence microscopes, AFMs do not create 2D images. AFM is a type of Scanning Probe Microscopy (SPM), which use a physical probe to scan the data and create surface images. In AFM, the physical probe is a very sharp and small tip. This tip mechanically moves over the surface and scans it line by line, and eventually an image is created by considering the force of tip-surface interaction. The resolution of AFM is smaller than a nanometer, and much better than that of fluorescence microscopes.

In [Fronczek et al.]'s work, Fluorescence and AFM images of the same sample area are obtained separately and the centers of quantum dots (fiducial marker particles that provide point light sources) visible in both types of images are localized. These centers provide the anchor points for image registration; so that in the resulting hybrid images, a fluorescence signal marks and unambiguously identifies specific fluorescently-labeled protein molecules in the topographic AFM images (see Figure 1).

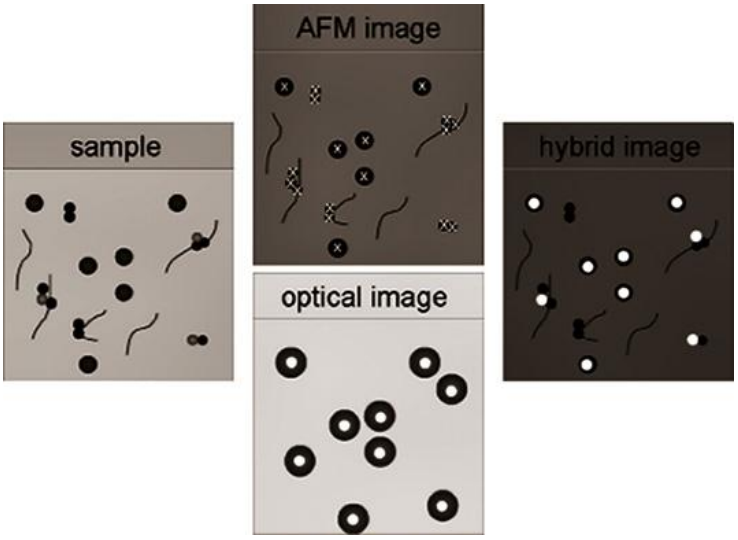

Figure 1. A sample of protein 1 (small black filled circles) and fluorescently labeled protein 2 (small light gray filled circles) that form multi-protein complexes on DNA (black lines) is imaged by AFM and by fluorescence microscopy. Quantum dots (large black filled circles) are added to the sample to provide fiducial markers. Quantum Dots have distinct signals in both the topographical AFM and the fluorescence (i.e. optical) images. Center fitting algorithms are applied to the markers in the AFM and fluorescence images, separately (white crosses in AFM image, white filled circles in optical image). At the end images are aligned (based on corresponding locations of the markers) to come up with a hybrid image.

The processing of the individual fluorescence and AFM images as well as the exact registration (with nanometer accuracy) of the separate types of images of the same sample area is essential to localize the correct molecule in the hybrid images. Highly accurate image registration requires three separate steps of data processing:

(1) Precise localization of particle centers in the fluorescence images
(2) Precise localization of particle centers in the AFM images
(3) Accurate overlay of these centers through an affine alignment of the two images

Software related to part (1) and (2) has been integrated to [Taylor et al.]'s NanoManipulator by Cory Quammen. In these steps, the user gives initial starting points for the location of the markers, and then the optimization is done by the algorithm chosen by the user (Details on the optimization methods are given in section 4.1).

In my work, I focused on the automation of initial point finding (related to points 1&2 above) and automation of the registration process (point 3 above).

2. Problem Statement

Figure 2.1 is an AFM image with heights mapped to brightness, and Figure 2.2 is a corresponding fluorescence image of the same specimen. Even for biologists, it is a cumbersome –if not impossible- task to manually find correspondences in an AFM-fluorescence image pair like this. The aim here is to *register* these two images. *Image registration* is the process of transforming different images into a single coordinate system.

The manual image registration process takes many hours of work depending on the number of markers visible in each image. Dr. Tessmer and her group at the University of Wuerzburg had tried many AFM-fluorescence image pairs for the [Fronzcek et al.] paper. A successful manual alignment took them half a day. In other cases, they were not even able to do the alignments. Here are the reasons they mentioned:

- Users can quickly find the correlations when there are preattentive features (i.e. features that can be detected by humans without focused attention) in the image. However, there are no preattentive features in image pairs most of the time.
- The number of markers is generally on the order of hundreds. When the user finds a small number of matching point couples, she starts to find neighbors of these matching points by considering relative positions of these neighboring markers to the matching points, which soon leads to losing track of the process.
- Most of the time, there are numerous similar-looking patterns in the images, which is misleading for the user.

Apart from the large number of visible markers in each image, there are other important issues:

- AFM and fluorescence images do not cover the same portion of the data. That is, one image can be a subset of the other image in terms of the region it covers.
- The images may be rotated, scaled, or flipped.
- Due to unavoidable characteristics of the experiment and sample, markers can be missing in images. It may be the case that a marker is visible in the AFM image but is invisible in the fluorescence image, or vice versa.

Figure 2.1: An AFM image, where the markers are seen as white dots

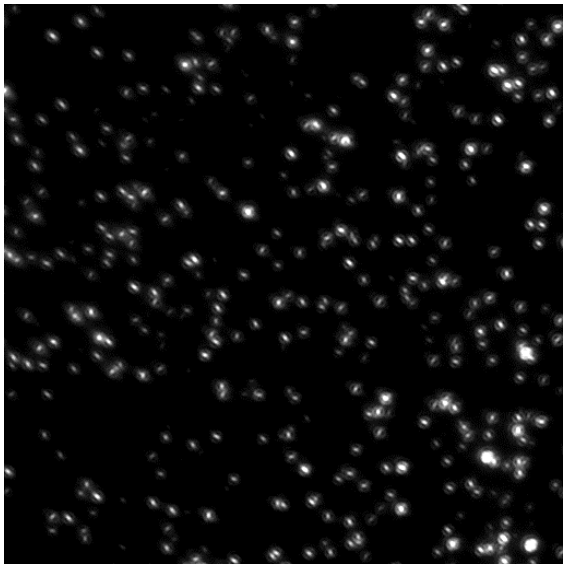

Figure 2.2: A fluorescence image from the specimen used in Figure 2.1

3. Background Research

The problem that I have worked on can be divided into two main parts. The first part is finding the fiducial markers in the AFM and fluorescence images. Once the markers are located, we go to the second part, which is registering the AFM-Fluorescence images. Before explaining how I approached the problem, I will give some background information about two image registration methods that have similarities to my image registration method.

3.1 RANSAC

A commonly used method to fit a model to a set of data with outliers is a non-deterministic algorithm called RANSAC (Random Sample Consensus), devised by [Fischler and Bolles]. RANSAC is used in several Computer Vision problems. One type of problem is related to image registration, where we try to merge two or more images that partially overlap (For the sake of simplicity, I will assume that we only have two images for the rest of the section). In this kind of problem, before running RANSAC, we find the data points in the images, and then we find the point-pairs from our images that are similar to each other. This operation is called "feature-matching", since it is done by comparing markers' feature descriptors that are defined using pixel value information around the markers. Having features matched does not imply that our registration problem is solved. There can be many outliers among the matches (Similar-looking descriptors may be coming from different regions in the data); but this step still narrows down the search space hugely.

After we have these matches with many outliers, we run RANSAC on them:

X := $\{x_1, x_2, x_3, \ldots, x_n\}$ where n is the number of correspondences (point pairs). We want to fit a model to X using m correspondences out of n correspondences, where $m \leq n$.

K := The number of iterations that the algorithm is going to take.

T := The tolerance value. A correspondence is considered as valid if it the distance between itself and the defined model is less than T (the distance between the actual location of the point in the image that we are projecting the other image into and the projection of its matching point).

S := The size of the consensus set that the number of valid correspondences (inliers) should reach to confirm the calculated model as sufficiently good.

for iteration_count := 1 to *K-1*

Pick m correspondences randomly out of X.

Compute a model using the picked correspondences.

Determine how many correspondences in X are closer than T to the model: If the number is bigger than or equal to S, recompute the model based only on the valid correspondences.

end

Accept the model with the biggest S value.

The nice part about RANSAC is that, unlike using least-squares on data points for model fitting, it is resistant to outliers. The reason is that, during model-fitting, only the correspondences that look promising to be inliers (i.e. "valid correspondences" in the algorithm above) are considered, and correspondences that are likely to be outliers are not taken into account.

If there is an affine transformation between images, we can select *m* as small as 3 (i.e. 3 pairs of points). A point-pair is assumed valid if the distance between a point in the pair that was projected to the other image and the actual location of the other point in the pair is less than *T*. However, in our case of AFM-fluorescence images, there are no feature descriptors that can be defined from pixel values since all markers in AFM and all markers in fluorescence image look similar to each other (there are no characteristic differences between markers in an image) and the imaging techniques used are different (different microscopes). Because of this reason, we do not have feature-matches, which means that there are no pre-estimated point matches that we can use to judge point projections as valid or invalid.

A lot of research has been done on tuning the parameters (*K, T,* and *S* above), which is the most critical part. The idea depends on probability, which means that we can never guarantee that we have the best possible registration. In addition, since the points are picked randomly, we may have different solutions in different runs of the algorithm. In section 5, I will show that my algorithm narrows down the search space further and then compares every possible combination, which means that it always finds the best (and same) possible solution in different runs.

In RANSAC, it can also be the case that the calculated registration does not fit the data at all. If the parameters are not well defined, the chance of this happening is larger. As I will mention later in section 5, one good part about my algorithm is that we do not have any parameter tuning.

Apart from picking *m* initial point pairs randomly rather than deterministically, the loop shown above does the same operations in my algorithm in section 5 at each operation. The number of expected number of iterations *K* to select *m* good data points using RANSAC can be calculated as follows [Fischler and Bolles]:

- E(k) is the expected value of *K*
- $b = w^m$ (*w* is the probability of having a randomly selected point-pair be a "valid" one)
- $a = (1-b)$
- x_i is the number of iterations it takes to find a set with only inliers; and p_i is the probability that we come across to a set of only inliers in one of the iterations.

$E(K) = \sum_{i=1}^{\infty} x_i p_i = \sum_{i=1}^{\infty} i p_i$

$E(K) = b + 2*(1-b)*b + 3*(1-b)^2*b + \ldots + i*(1-b)^{(i-1)}*b + \ldots$

$E(K) = b*[1 + 2*a + 3*a^2 + \ldots + i*a^{(i-1)} + \ldots]$

Using infinite geometric series progression, we know that:

$a + a^2 + a^3 + \ldots + a^i + \ldots = \frac{a}{1-a}$

When the above formulation is differentiated with respect to *a*:

$1 + 2*a + 3*a^2 + \ldots + i*a^{i-1} + \ldots = \frac{1}{(1-a)^2}$

This gives us:

$E(K) = b*[1 + 2*a + 3*a^2 + \ldots + i*a^{(i-1)} + \ldots] = b * \frac{1}{(1-a)^2} = b * \frac{1}{b^2} = \frac{1}{b} = w^{-m}$

As mentioned above, if we assume an affine transformation, we can pick *m* as 3. In our AFM-fluorescence images, since we do not have any feature-matches, the space of point-pairs that one should search through is *q*r*, where *q* is the number of markers in the AFM image and *r* is the number of markers in the fluorescence image. If we calculate the transformation from AFM to fluorescence image, then *w* is *q/(q*r)*, which is 1/*r.* Considering the fact that we have hundreds of markers in both images, w^{-m} can be on the order of millions. In my algorithm, we will see that we only iterate the loop "*q"* times. So, if these two methods are compared, we have:

$w^{-m} = r^m$ iterations (from RANSAC) versus q iterations(from my algorithm)

Both r and q are on the order of hundreds, so:

$O(r^m)$ vs $O(q)$ ≈ $O(q^m)$ vs $O(q)$ = $O(q^3)$ vs $O(q)$

which means that we have cubic reduction in runtime.

3.2 Astrometry

If we move from nanometer scale to the size of the observable universe (on the order of 10^{10} light years), we see a similar problem to our task of AFM-fluorescence image alignment. In the astrometry (i.e. the scientific area on determining positions of stars and other celestial bodies) literature, one common issue is recovering the position of stars in a given astronomical image by matching it to a universal database of stars (The database is put into a search tree beforehand). [Lang et al.]'s work is a good reference for this topic. As in the case of AFM and fluorescence images, there are no feature descriptors in the astronomical images that come from pixel values: The only visible features are stars. Another similarity of [Lang et al.]'s work to our problem is that some stars may be missing in an astronomical image that will be searched through the universal database.

To create feature descriptors that are invariant to rotation, translation, and scale, [Lang et al.] take nearby quadruples of stars and define a local coordinate system for each quadruple. To define a local coordinate system, they find the most widely separated star pair in the quadruple, and set one star in the pair as origin (0,0), and the other as (1,1). Then, the coordinates of the remaining two stars are calculated in this local coordinate system. In this way, they create a descriptor that gives relative positions of the four stars (Figure 3). They do the same operations to most of the nearby quadruples of stars in the image, and then find candidate regions in the universal database by matching the descriptors in the image and the database. Once the candidate regions are found, each candidate is aligned with the astronomical image by transforming it using one of the common quadruples, and the candidate that fits best to the image is picked as the correct region.

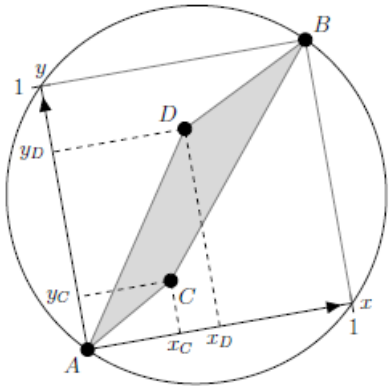

Figure 3: This figure is from [Lang et al.]'s paper. Here, we see the descriptor for a quadruple of stars, A, B, C, and D. Star A defines the origin and star B is at location (1,1) in a local coordinate system. In this local system, the positions of stars C and D are computed. The coordinates (x_C,y_C) and (x_D,y_D) are used to form the descriptor (x_C,y_C,x_D,y_D) for the relative positions of the four stars. The descriptor is invariant under translation, scaling, and rotation of the four stars. Swapping A and B converts the descriptor to $(1- x_C, 1- y_C, 1- x_D, 1- y_D)$.

In section 5, I will show that my algorithm can be considered as a combination of the ideas from [Fischler and Bolles] and [Lang et al.]. As in the case of [Lang et al.], I used a descriptor model that is calculated via relative positions of points to each other. Once I have feature descriptors, the rest is just like RANSAC except I consider every point-set rather than a random subset and hence there is no related parameter tuning. Since the number of iterations to be taken in my algorithm is equal to *a (i.e.* the number of markers in AFM image, which is on the order of hundreds), there is no need to use a non-deterministic method since the complexity is linear (i.e. O(*a*)) in terms of iteration count, which means that we can run a deterministic algorithm that always finds the best possible model by testing all feature-matches in a very short period of time (less than a second).

4. Finding Markers Automatically

4.1 Fluorescence and Undistorted AFM Images

In [Fronczek et al.]'s work, center fitting algorithms for subpixel accuracy were applied after manually picking initial locations for the markers. If there are not many markers to pick (e.g. in Figure 4.1), it may not be a hard task for the user to manually select them one by one. However, it may be a cumbersome task for the user if there are a lot of markers to select (e.g. in Figure 4.2). In any case, users prefer an unbiased automatic algorithm. I developed such an algorithm.

An intensity threshold-based segmentation was defined for the AFM and fluorescence images separately. The idea is to reject markers that have a lower intensity value than the intensity threshold decided by the user. By using a threshold, the user is able to eliminate points which may look like markers but are just noise/background in reality.

The algorithm finds pixels that are above the user-defined threshold, and eliminates the ones that are too close (less than the average marker-size away) in order to assign one pixel per marker.

Once the initial marker positions are found using my algorithm, existing local-center fitting algorithms locate these markers to subpixel accuracy. Center fitting is done with a local maximum tracker for the AFM image, and with a FIONA tracker for the fluorescence image.

In their paper, [Fronzcek et al.] show that markers in the fluorescence image can be approximated using Gaussian distributions. By convolving 2D-Gaussian functions to the markers using FIONA tracker, they find the center locations of these markers typically within 10 nanometers. Using local maximum fitting in fluorescence images was not preferred, because it gives the pixel with local maximum intensity as the center of the marker, which means that localization can be as bad as half the fluorescence image pixel size (i.e. 34 nanometers).

The local maximum tracker selects the position of the pixel with maximum height as the particle center. Unlike the case with optical image markers, AFM markers do not have Gaussian distributions, since the specimen is mechanically scanned. The worst localization accuracy using local maximum fitting can be half the AFM pixel size, which is 8 nanometers.

The results of running my algorithm are shown in Figure 4.1 and Figure 4.2.

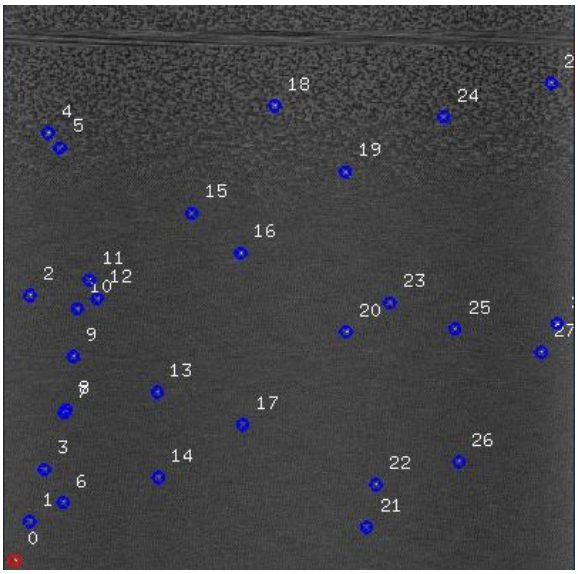

Figure 4.1: Markers automatically found in an AFM image

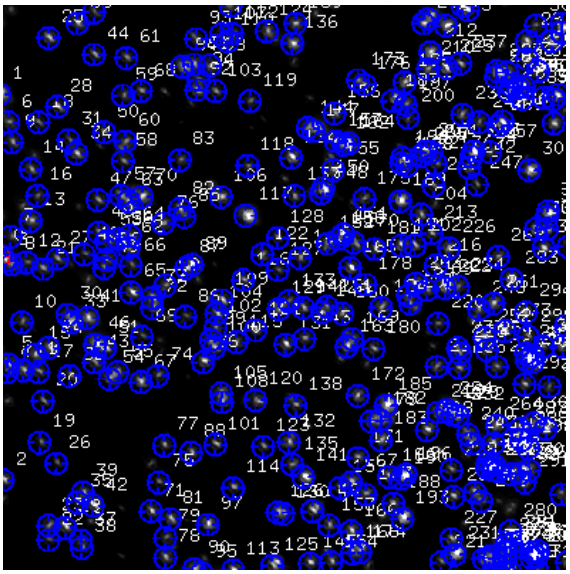

Figure 4.2: Markers automatically found in a fluorescence image

4.2 Distorted AFM Images

Because of imperfections in the AFM scanner, the image can get distorted. In a distorted AFM image, a flat surface is unwantedly mapped to a semi-cylindrical surface where the regions on the sides of the image are at a higher position than the actual and the center of the image in a lower position than the actual, or vice versa. When this data is visualized by mapping height values to grayscale values (where a higher point maps to a brighter pixel), we have a bright region surrounded by darker regions (see Figure 5), or vice versa. Because of this fact, if we use a global intensity threshold like in 4.1, we either miss markers (when we use a higher threshold), or pick all the markers along with many pixels that are not actual markers (when we use a lower threshold).

Dr. Wu from Prof. Erie's lab at UNC Chemistry told me that he had distorted AFM images in his experiments. For dealing with the problem, two different options were considered:

A) Calculating a mapping from the distorted surface to an undistorted surface

B) Calculating local maximum pixels rather than setting a global intensity threshold

To have a user-friendly system, it is ideal to have a global method that can work for any given distorted AFM image. Option A is a model-based method. The idea in this option is to find a global model, and then to apply the method mentioned in 4.1 to the newly-derived undistorted image. The mechanical AFM tip may not behave the exact same way at each run, which means that the distortions for different runs may be different. Although this does not directly point to the lack of a global model definition that would transform any distorted AFM image to undistorted versions, it makes finding such a model a complex task. In other words, the global model, if it exists at all, is not known (It is important to clarify at this point that the distortion is only on the z-axis; that is, only the heights of the pixels are different than their corresponding undistorted versions).

Unlike option A, option B is a non-model-based method. In this option, we define a sliding window over the image. At each location of the window, we pick the pixel at the center of the window as a valid marker if the pixel has an intensity value several standard deviations higher than the mean of the pixels on the edges of the given window. The calculation is not specific to a given distortion but rather can be applied to any distorted image. The only possible disadvantage of option B compared to option A could be having a noisier marker finding since we do not project each pixel to its undistorted version. However, since our markers are always much brighter than their local surroundings (i.e. brighter than the pixels on the edges of defined sliding windows), we do not have the problem of picking the wrong pixels. Figure 5 shows the difference between using global intensity and using option B on a distorted image.

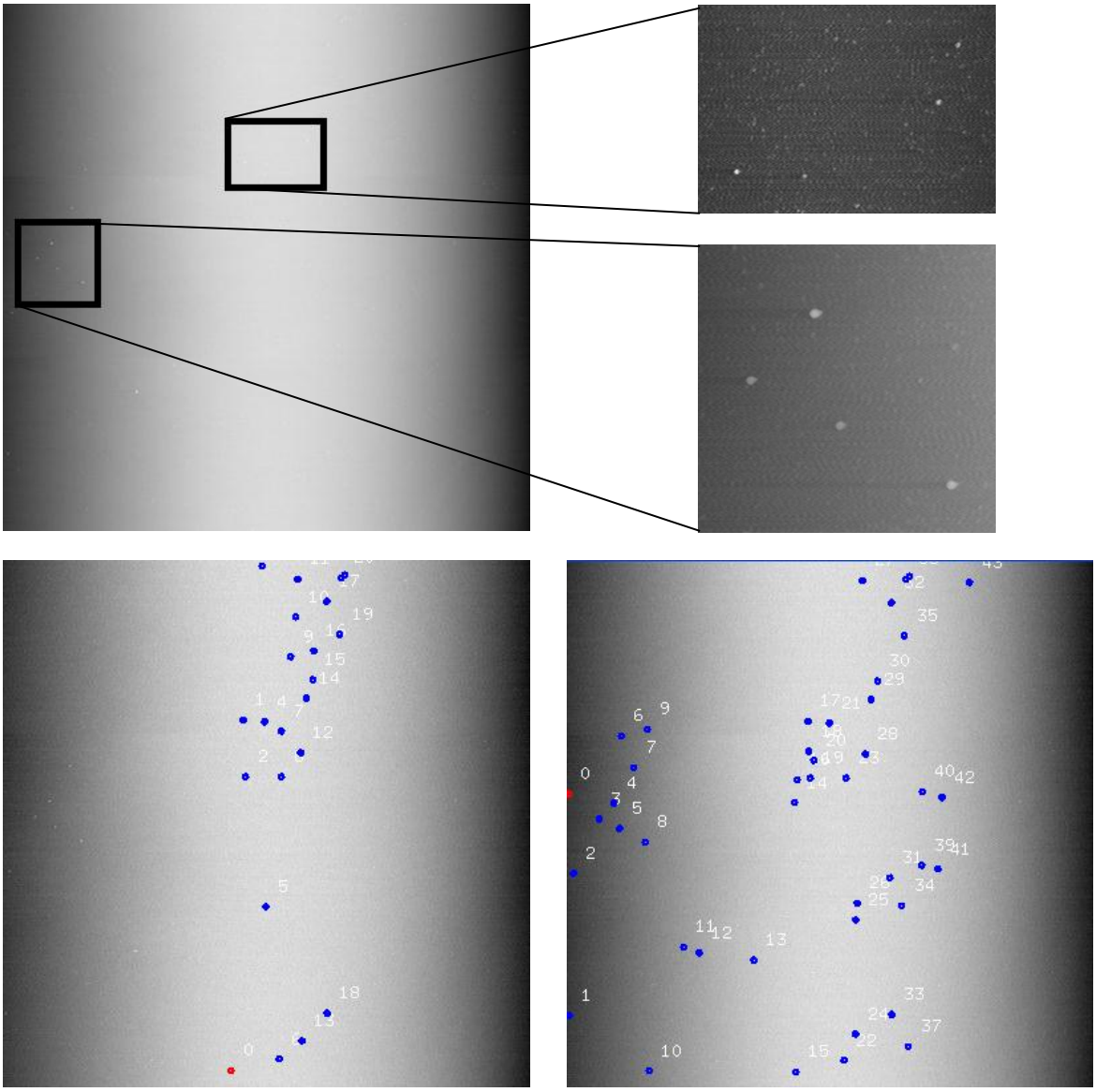

Figure 5: On top-left, we have a distorted image where the brightest region is in the middle and it gets darker to the left and right edges. On top-right, there are two close-ups from two different regions: one from the darker region, one from the brighter region (Color properties of these close-ups have been manipulated here to make all of the markers visible to the reader). Because of the distortion, if we use a global intensity threshold, either only markers from the bright area would be chosen (when the threshold is high [as seen in the bottom-left image]), or all the markers in the image with lots of false positive points would be chosen (when the threshold is low). Instead, when we calculate local maximum pixels with a defined local window and pick the local maximum pixels that are several standard deviations higher than the mean of the pixels on the edges of the given window, we find markers throughout the image (bottom-right).

5. Automatic Registration of AFM-Fluorescence Image Pairs

After initial marker coordinates for AFM and Fluorescence images are produced (either manually or automatically as described in section 3.1), automated registration between AFM images and optical images can be calculated.

While my algorithm is strictly speaking designed to recover similarity transforms only, experimental evidence indicates that the AFM/fluorescence transformations are sufficiently close to similarity transforms which allows the application of my algorithm. According to this, an image can be projected to the other image by a combination of translations, rotations, and changes of scale. In order to find the coefficients of the matrix that describes the transformation for an image pair, using three pairs of corresponding markers is sufficient.

The registration algorithm is as follows:

- For each marker in the AFM image, find its two nearest neighboring markers (using Euclidean distance).

- For each marker in the Fluorescence image, find its two nearest neighboring markers (using Euclidean distance).

- For each marker triplet in each image (i.e. a given marker and its two nearest neighbors), calculate the ratio of distances of neighboring markers to the marker of interest. Save the ratio as “d1/d2”, where d1 is the distance from the marker to its nearest neighbor and d2 is the distance to its second nearest neighbor.

- For each triplet in the AFM image, find triplets in the Fluorescence image which have similar ratios (Due to using two different imaging techniques, corresponding markers from AFM and fluorescence images cannot be exactly overlaid, so the algorithm accepts distance ratios that do not differ by more than a small threshold).

- For each candidate match, calculate the affine transformation matrix, and apply this matrix to every marker in the AFM image, which maps the points in the AFM image to the Fluorescence image.

- For each transformation matrix coming from a candidate match, calculate the median distance to the nearest points and assign it as the error of the transformation (figure 6).

- At the end of all iterations, pick the transformation which gives the least median error.

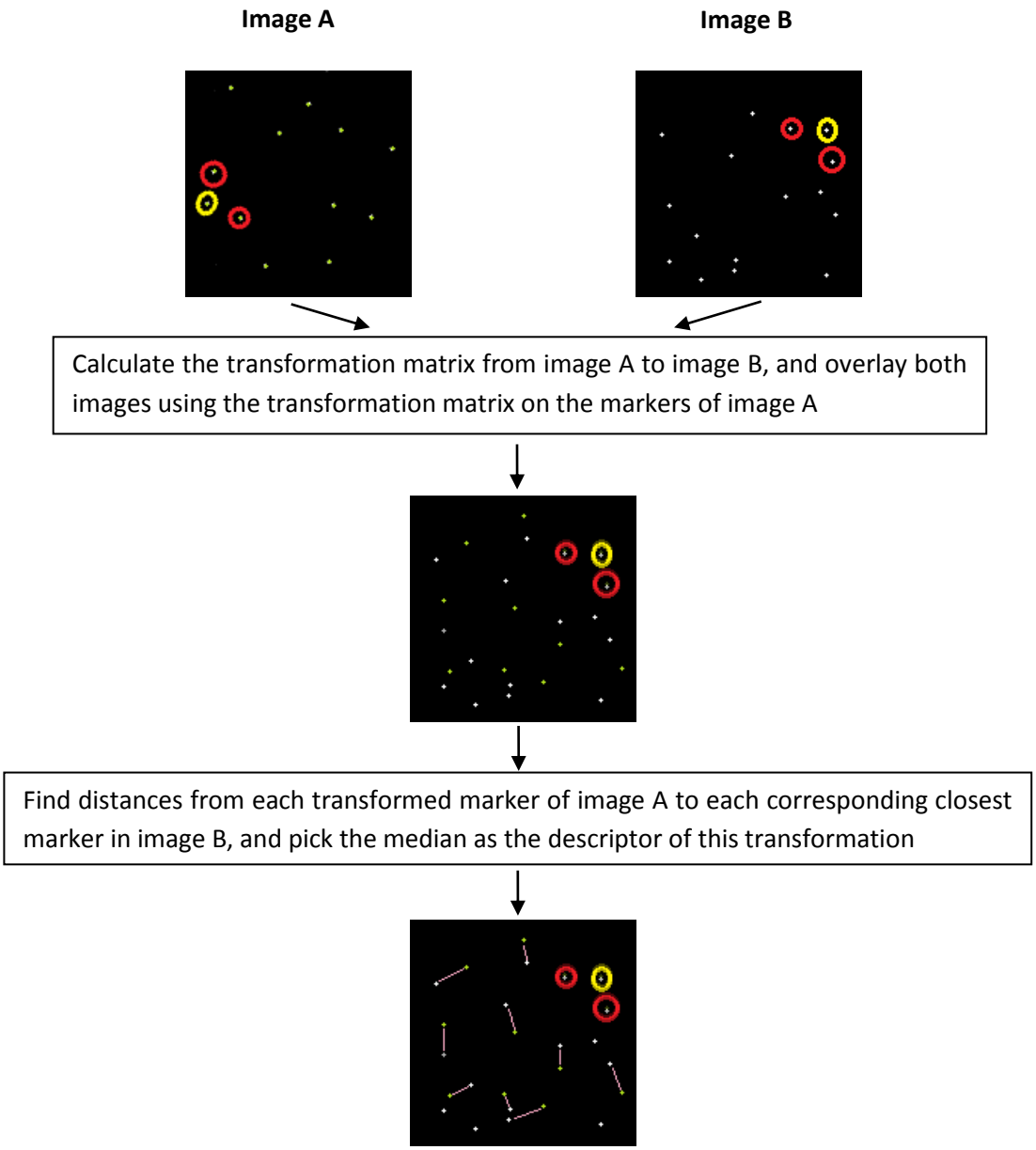

Figure 6: Outline of a single iteration of the algorithm where a triplet is found in image A that has a similar ratio with a triplet in image B. The markers encircled with yellow are the main markers of the triplet, whereas the ones encircled in red are the nearest neighbors to the ones in yellow. Markers of image A are shown in green, and markers of image B are in white. Once the overlay is done according to these highlighted triplets by calculating the related transformation matrix, the median distance value is saved as the penalty score of the transformation.

6. Results

To test the consistency of the automated registration algorithm, I first derived artificial datasets. I created an artificial specimen, and then from this specimen, I derived other specimens, each of which was gotten by applying to the main specimen a single aspect of affine transformation (i.e. rotation, translation, scale, flipping), or a combination of different aspects of affine transformation. By doing this, every possibility that can arise with an affine transformation was covered. Without considering the case of missing points in images, I got correct automatic registration in every experiment.

One important problem in actual datasets is missing markers (both in AFM images and fluorescence images). Starting with testing combinations of aspects in affine transformation without any missing markers, I gradually increased the rates of missing markers in both images by randomly deleting markers from each image. In theory, the power of the algorithm is the guarantee that it will work if a triplet of markers (a given marker and its two closest neighbors) is seen in both AFM and fluorescence images, no matter what happens to the other markers in our images. With randomly deleted points in both images, I got correct automatic registration up until the point where 50% of the markers in AFM and fluorescence images were missing. In all cases, automatic registration took less than a second.

After getting correct results with artificial specimens, I tested the automated registration algorithm on real specimens gotten from scientists (an example is seen in figures 7.1, 7.2, and 7.3). There were four AFM-fluorescence pairs in total on which the tests were done. In three of them correct overlay was gotten. However, in one AFM-fluorescence pair, the algorithm failed and gave a completely incorrect registration. A possible reason for this may be having many missing markers in at least one of the images (AFM or fluorescence) such that no marker triplets from immediate neighbors exist; which means that the algorithm cannot work. For the image pair which my algorithm wasn't able to register, the scientists were also unable to come up with a manual registration.

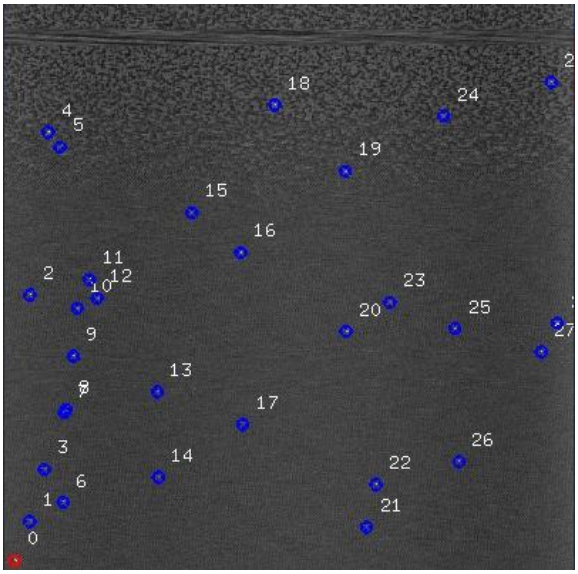

Figure 7.1: These are the markers previously found in automatic point finding stage. During registration, these AFM markers are mapped into the fluorescence image.

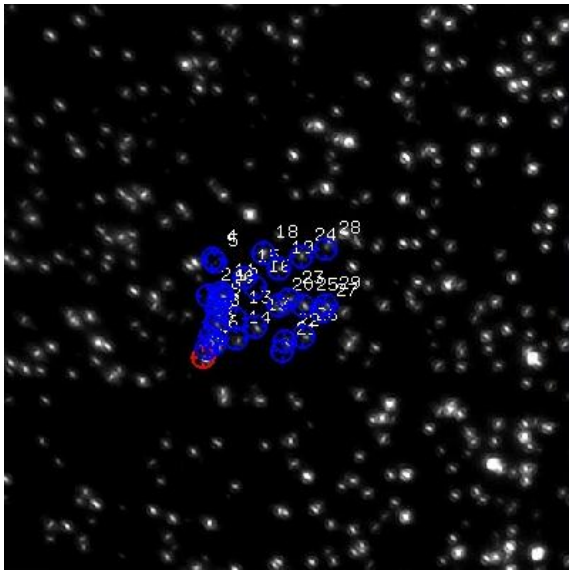

Figure 7.2: Corresponding locations of the markers that were mapped from the AFM image to the fluorescence image.

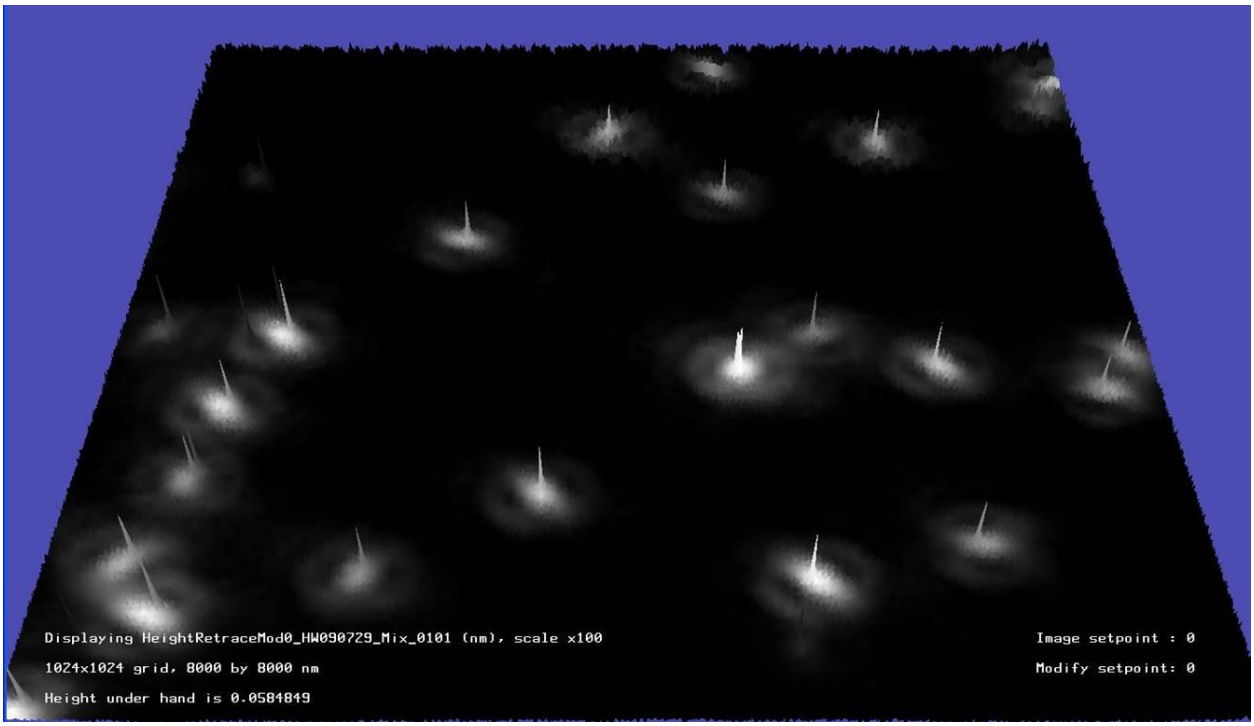

Figure 7.3: Overlay of two images. Topography is coming from the AFM images, whereas the colormap is coming from the fluorescence image. Seeing many bright “hills” means that the alignment was successful.

7. Conclusion

I applied marker finding and automatic registration methods on Dr. Tessmer's images from her system that uses fluorescence microscopy and AFM on the same specimen. This reduced the time that the scientists spare for these operations from many hours (in the case of using manual methods) to seconds and its error is smaller.

8. Future Work

In some of his experiments, Dr. Wu is using a type of quantum dot that has higher probability of not being seen at a given instant. In his experiments, the number of markers seen in the fluorescence image is as low as 3-4, and the number of markers in the AFM image is generally between 40 and 50. However, unlike our case where markers were also missing in the AFM image, in his experiments, all of the markers in the AFM image are visible.

My algorithm would not work in this circumstance, since there is no triplet in the fluorescence image that consists of immediate neighbors. But since the search space is very small, we can try every possible triplet in the AFM image (not just the ones consisting of immediate neighbors, but every possible combination) against every possible triplet in the fluorescence image. Dr. Wu is currently working on creating specimens that I can work on.

9. References

Fischler, M. A., Bolles, R. C. “Random sample consensus: A paradigm for model fitting with applications to image analysis and automated cartography,” Communications of the ACM, Volume 24, Pages 381-395, June 1981.

Fronczek, D.N., Quammen, C., Wang, H., Kisker, C., Superfine, R., Taylor, R., Erie, D.A., Tessmer, I. “High accuracy FIONA-AFM hybrid imaging”, Ultramicroscopy, Volume 111, Issue 5, Pages 350-355, April 2011.

Lang, D., Hogg, D. W., Mierle, K., Blanton, M., Roweis, S. “Astrometry.net: Blind astrometric calibration of arbitrary astronomical images”, The Astronomical Journal, Volume 137, Pages 1782–1800, 2010.

Taylor, R. M., Robinett, W., Chi, V. L., Brooks, Jr., F. P., Wright, W. V., Williams, R. S., and Snyder E. J. “The Nanomanipulator: A Virtual-Reality Interface for a Scanning Tunneling Microscope”, Computer Graphics: Proceedings of SIGGRAPH '93 , August 1993.

Tessmer, I. “Single molecule studies of DNA repair”.
http://www.virchow-zentrum.uni-wuerzburg.de/forschung_en/index.php?rubric=tessmer_en